CHEMISTRY
AN ASIAN JOURNAL

www.chemasianj.org

A Journal of

ACES
Asian Chemical Editorial Society

A sister journal of **Angewandte Chemie** and **Chemistry – A European Journal**

WILEY-VCH

Synthesis of Pd-Pt Ultrathin Assembled Nanosheets as Highly Efficient Electrocatalysts for Ethanol Oxidation

Yeji Han,[a] Jeonghyeon Kim,[b] Su-Un Lee*,[c] Sang-Il Choi,*[b] and Jong Wook Hong*[a]

[a]Department of Chemistry, University of Ulsan, Ulsan 44610, South Korea.

[b]Department of Chemistry and Green-Nano Materials Research Center, Kyungpook National University, Daegu 41566, South Korea.

[c]Carbon Resources Institute, Korea Research Institute of Chemical Technology, 141, Gajeong-ro, Yuseong-gu, Daejeon 34114, South Korea.

*Correspondence and requests for materials should be addressed to J.W.H., S.-I.C., and S.-U.L. (email: jwhong@ulsan.ac.kr; sichoi@knu.ac.kr; sulee@krict.re.kr)

Abstract

Control over composition and morphology of nanocrystals (NCs) is significant to develop advanced catalysts applicable to polymer electrolyte membrane fuel cells (PEMFCs) and further overcome the performance limitations. Here, we present a facile synthesis of Pd-Pt alloy ultrathin assembled nanosheets (UANs) by regulating the growth behavior of Pd-Pt nanostructures. Iodide (I^-) ions supplied from KI play as capping agents for the {111} plane to promote 2-dimensional (2D) growth of Pd and Pt, and the optimal concentrations of cetyltrimethylammonium chloride (CTAC) and ascorbic acid (AA) result in the generation of Pd-Pt alloy UANs in high yield. The prepared Pd-Pt alloy UANs exhibited the remarkable

1

enhancement of the catalytic activity and stability toward ethanol oxidation reaction (EOR) compared to irregular-shaped Pd-Pt alloy NCs (IS NCs), commercial Pd/C, and commercial Pt/C. Our results confirm that the Pd-Pt alloy composition and ultrathin 2D morphology offer high accessible active sites and favorable electronic structure for enhancing electrocatalytic activity.

KEYWORD: Pd-Pt bimetallic, Nanosheet assembly, Ethanol oxidation reaction,

2

Polymer electrolyte membrane fuel cells (PEMFCs) are efficient energy converting systems that operate based on the electrooxidation of fuels.[1-4] PEMFCs potentially have high energy and power densities, but fall short of expectations due to the lack of high-performance electrocatalysts.[5] Pt has been accepted as the most efficient catalyst for fuel oxidation reactions,[6-9] but has the disadvantages of high cost and low-reserves.[9-11] In addition, its insufficient activity and poor stability due to the poisoning by reaction intermediates and deformation of catalysts are also considered as limitations for practical application.[12-14] An effective strategy for improving the activity and stability of Pt is alloying it with other metals, such as Pd, Ir, Ru, Au, and Pb.[15-19] Introducing the secondary metal component can modulate the electronic structure of Pt and thus weaken the affinity of poisoning species.[20] In particular, Pd is a promising candidate to form a strong coupling with Pt and synergistically enhance the catalytic properties due to the same face-centered cubic (fcc) structure with a highly similar lattice constant of nominal mismatch of 0.77%.[6,21,22]

As an another approach to enhance the electrocatalytic performance, preparing nanocrystals (NCs) can offer an advantage for increasing high accessible active sites participating in the electrocatalytic reaction due to their large surface area to volume ratio as compared with bulk materials.[23] Notably, metal ultrathin assembled nanosheets (UANs) composed of multiple ultrathin nanosheet subunits are one of efficient nanostructures that can maximize surface area to volume ratio.[24-27] For example, Pi *et al.* reported that Ir UANs exhibited larger catalytic activity compared with irregular-shaped 3-dimensional (3D) Ir NCs for oxygen evolution reaction (OER).[27] However, synthetic conditions for achieving the UANs are strict because the in-plane growth rate should be sufficiently fast by effectively suppressing the out-of-plane growth of the metal. Since it is difficult to simultaneously control in-plane and out-of-plane

3

growth kinetics, typical 3D metal nanostructures are produced under common synthetic conditions. Therefore, the synthesis of metal UANs has attracted significant interest in recent years for the preparation of highly challenging and efficient electrocatalysts.

Herein, we report the facile synthesis of Pd-Pt alloy UANs by co-reduction of Pd and Pt precursors. In our synthetic route, the iodide (I⁻) ions as the stabilizing agent play a key regulator for developing the UAN structure. In addition, growth rate of the UANs can be modulated by adjusting the amounts of cetyltrimethylammonium chloride (CATC) and ascorbic acid (AA) used as stabilizer and reductant, respectively. The Pd-Pt alloy UANs exhibited highly enhanced electrocatalytic activity and stability toward ethanol oxidation reaction (EOR) compared with Pd-Pt alloy irregular-shaped NCs (IS NCs), commercial Pd/C, and Pt/C owing to the synergistic advantages by Pd-Pt alloy component and unique morphology.

The Pd-Pt alloy UANs were synthesized by reducing K_2PdCl_4 and K_2PtCl_4 in an aqueous solution containing KI, CTAC, and AA as a capping agent, a stabilizer, and a reductant, respectively. Figure 1a,b and Figure S1 display representative scanning electron microscopy (SEM) and transmission electron microscopy (TEM) images of the products, demonstrating that they are composed of several 2D nanosheets and each nanosheet subunit is interconnected by sharing edges. Weak contrasts at subunit parts in the UAN indicate the ultrathin thickness. The small spherical NCs with an average diameter of 4.2 nm were loaded on the nanosheet subunits (Figure 1c). The fast Fourier transform (FFT) pattern obtained from a nanosheet subunit confirms the highly crystalline nature of the products (the inset of Figure 1c). The thickness of the nanosheet subunits of UANs was estimated to be approximately 6.0 ± 0.5 nm measured by high resolution TEM (HRTEM) image taken from the side plane (Figure 1d).

For an investigation of the detailed compositional characteristics of the UANs, elemental

4

mapping images were obtained by using high angle annular dark field scanning TEM−energy-dispersive X-ray spectroscopy (HAADF−STEM−EDS) measurement (Figure 2), which clearly confirms the formation of a homogeneous Pd-Pt alloy structure. Furthermore, HRTEM image in the inset of Figure 1c reveals the lattice spacing of 2.24 Å, which corresponds as the (111) planes of fcc Pd-Pt alloy.[6,28] The Pd/Pt atomic ratio of the Pd-Pt UANs was determined as 10:1 by inductive coupled plasma-optical emission spectroscopy (ICP−OES). For X-ray diffraction (XRD) pattern of the Pd-Pt alloy UANs (Figure S2), the representative diffraction peaks of the (111), (200), (220), and (311) planes were detected at 40.0, 46.5, 68.1, and 82.1° between the positions expected to pure Pd and Pt, indicating the formation of Pd–Pt bimetallic feature.

For the formation of the Pd-Pt alloy UANs, the concentrations of I⁻ ions, CTAC, and AA are critical factors to control the growth behavior of Pd and Pt. To investigate the influence of concentration of I⁻ ion, different amounts of KI ranging from 0 to 36.50 mM were used under otherwise identical conditions for standard UANs. When 0, 3.29, 6.17, and 10.99 mM of KI were introduced instead of standard KI concentration (18.02 mM), irregular-shaped nanostructures were obtained (Figure S3a-d), while introduction of KI from 18.02 to 22.90 mM produced the nanostructures with assembled nanosheet shapes (Figure S3e,f). It is noted that the shape and size of the NCs formed in 3.29 mM of KI were similar with those of spherical NCs (4.2 nm) on the Pd-Pt alloy UANs produced by 18.02 mM KI. Based on this finding, we believe that the formations of spherical NCs and nanosheets are competitive in our synthesis condition. The 18.02 mM of KI can dominantly lead to the formation of nanosheets by passivating the {111} facets of Pt-Pd. However, the small spheres were still formed on the surface of Pt-Pd UANs, indicating that suppressing the formation of Pt-Pd spheres were not

5

perfectly achieved.

However, the addition of 26.49 and 36.50 mM of KI induced the aggregated nanostructure (Figure S3g,h) because the excessive I⁻ ions in the reaction mixtures can cause the oxidative etching by halide ion/oxygen pairs.[29,30] These results unambiguously demonstrate that introducing the optimal amount of I- ions, which can effectively promote the 2D growth of Pd and Pt by suppressing the growth of [111] orientation and avoid unnecessary oxidative etching, is the primary prerequisite for the formation of the Pd-Pt alloy UANs. It is in good agreement with the previously reports that I⁻ ions are preferentially bound to the {111} crystal facet and facilitate the formation of anisotropic structures such as plates and prisms.[31] However, we found that I⁻ ion is not the only factor to determine the growth behavior of Pd and Pt, which was confirmed through a set of control experiments using different amounts of CTAC and AA. At lower amounts of CTAC (0.45 mM) or AA (0, 0.49, 1.21, and 2.36 mM) compared with those used in the standard synthesis nanosheets, highly similar shapes of nanostructures with standard Pt-Pd alloy UANs were developed (Figure S4a and Figure S5a-d); 2.27 mM of CTAC (Figure S4b) and 4.50 mM of AA (Figure S5e) were employed in the standard synthetic procedure for the Pd-Pt ultrathin assembled nanosheets, respectively. On the other hand, increasing the concentration of CTAC (4.55, 9.09, 22.73, and 45.45 mM) or AA (9.92, 16.56, and 24.88 mM) produced the 3D nanostructures with random sizes and shapes (Figure S4c-f and Figure S5f-h). These results can be interpreted that the capping effect of I⁻ ion is attenuated in the high concentration of CTAC and AA. The excess concentrations of CTAC and AA may disturb the adsorption of I⁻ ion on the surface of Pd-Pt nanostructures, and thus trigger the growth of 3D nanostructures with irregular shapes. On the basis of these results and findings, we found that I⁻ ions primarily facilitate the preferential 2D growth of Pd and Pt by being

6

passivated {111} plane and the adjustment of CTAC and AA concentration allows the production of Pd-Pt alloy UANs in high yield.

To investigate the morphological and compositional benefits from Pd-Pt alloy UANs, the EOR activity of the Pd-Pt alloy UANs supported on Ketjen black used as carbon support was evaluated in comparison with Pd-Pt alloy IS NCs loaded on the Ketjen black, commercial Pd/C, and commercial Pt/C catalysts. For the preparation of the Pd-Pt alloy IS NCs, two-times higher concentration of CTAC (4.55 mM) than that used for the synthesis of the Pd-Pt alloy UANs was introduced while other conditions kept the same as the preparation of the Pd-Pt alloy UANs. The elemental mapping images of the IS NCs exhibited that Pd and Pt signals are homogeneously dispersed through entire the NCs, demonstrating that compositional structure of the NCs is Pd-Pt alloy (Figure S6). The Pd/Pt atomic ratio of the Pd-Pt alloy IS NCs was determined as 10:1 by ICP-OES, similar to that of the Pd/Pt alloy UANs. Cyclic voltammograms (CVs) of catalysts are demonstrated in Figure 3a. Based on the integrated charges associated with cathodic peak between -0.54 and -0.10 V, the electrochemically active surface areas (ECSAs) of the Pd-Pt alloy UANs, Pd-Pt alloy IS NCs, Pd/C, and Pt/C catalysts were measured to be 27.7, 14.9, 30.4, and 31.2 $m^2\,g^{-1}$, respectively (Figure S7). The Pd-Pt alloy UANs showed roughly 1.9 times larger ECSA than the Pd-Pt alloy IS NCs due to their morphological benefit. Figure 3b shows the CVs obtained from the EOR of different catalysts in 0.5 M KOH and 1.0 M ethanol. The mass activities of the Pd-Pt alloy UANs, Pd-Pt alloy IS NCs, Pd/C, and Pt/C catalysts were 3369, 1510, 1430 and 1243 $mA\,mg^{-1}$, respectively (Figure 3b,d). Moreover, the analogous trend across the various catalysts was also obtained in the specific activity. The Pd-Pt alloy UANs, Pd-Pt alloy IS NCs, Pd/C, and Pt/C catalysts exhibited 12.16, 11.86, 4.71, and 3.99 $mA\,cm^{-2}$, respectively (Figure 3c,d). For both mass and specific

7

activities, the Pd-Pt alloy UANs and IS NCs showed the enhanced performances than commercial Pd/C, and Pt/C catalysts. This indicates that Pd-Pt alloy can effectively promote EOR than pure Pd and Pt surfaces. On the other hand, the higher activity of the Pd-Pt alloy UANs than that of the Pd-Pt alloy IS NCs obviously shows the larger ECSA of the Pd-Pt alloy UANs. Therefore, the significantly enhanced catalytic activity of the Pd-Pt alloy UANs is ascribed to the synergistic effects of Pd-Pt alloy and ultrathin 2D morphology, simultaneously leading to promote the intrinsic electrocatalytic properties and increasing the active sites.

Electrooxidation of ethanol in alkaline medium proceeds via the following ⅰ) reactive intermediate and ⅱ) poisoning intermediate pathway.[32, 33]

ⅰ) reactive intermediate pathway:

$M + OH- \rightarrow M\text{-}OH_{ads} + e^-$

$M + CH_3CH_2OH \rightarrow M\text{-}(CH_3CH_2OH)_{ads}$

$M\text{-}(CH_3CH_2OH)_{ads} + 3OH^- \rightarrow M\text{-}(COCH_3)_{ads} + 3H_2O + 3e^-$

$M\text{-}(COCH_3)_{ads} + M\text{-}OH_{ads} \rightarrow M\text{-}CH_3COOH + M$: rate determining step

$M\text{-}CH_3COOH + OH^- \rightarrow M + CH_3COO^- + H_2O$

ⅱ) poisoning intermediate pathway

$M + OH^- \rightarrow M\text{-}OH_{ads} + e^-$

$M + CH_3CH_2OH \rightarrow M\text{-}(CH_3CH_2OH)_{ads}$

$M\text{-}(CH_3CH_2OH)_{ads} + 3OH^- \rightarrow M\text{-}(COCH_3)ads + 3H_2O + 3e^-$

8
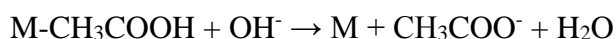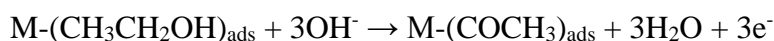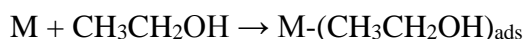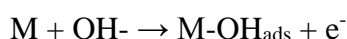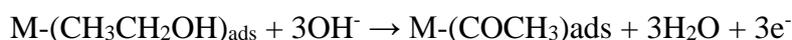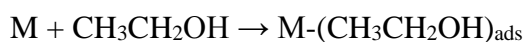
For reactive intermediate pathway, electrooxidation of $(COCH_3)_{ads}$ intermediate on the metal surface by reacting with OH_{ads} in the alkaline medium is the rate-determining step.[3,20] It has been previously reported that the up-shift of d-band center of Pd-Pt alloy surfaces compared with that of pristine Pd surface can promote the formation of OH_{ads} with optimal binding strength[34] and thus enhancement of EOR activity can be achieved on Pd-Pt alloy surface due to accelerated rate of $(COCH_3)_{ads}$ oxidation. To investigate the change in the electronic structure of the Pd-Pt alloy UANs, X-ray photoelectron spectroscopy (XPS) spectra of valence band regions were obtained and corresponding d-band center positions relative to the Fermi level were calculated. Indeed, the d-band center of the Pd-Pt alloy UANs was at -4.66 eV, which was -1.38 eV higher than that of Pd/C (Figure 4), which implies the up-shifted d-band center of the Pd-Pt alloy UANs. This can facilitate the formation of OH_{ads} on the Pd-Pt alloy than Pd surface, and thus transformation of $COCH_3$ to CH_3COOH on the catalysts (rate determining step) can be accelerated, boosting the EOR activity. Conclusively, the large surface area to volume by ultrathin assembled morphology and modified electronic structure of the UANs by alloying Pd and Pt can account for their enhanced electrocatalytic activity than pristine Pt and Pd catalysts.

The electrochemical stability of Pd-Pt alloy UANs was estimated by repeating CV and compared with Pd-Pt alloy IS NCs, Pd/C and Pt/C catalysts. Glassy carbon electrode (GCE) containing catalysts was applied between -0.9 and 0.3 V in N_2-saturated 0.5 M KOH and 1.0 M ethanol. After 300 cycles, the Pd-Pt alloy UANs, Pd-Pt alloy IS NCs, Pd/C, and Pt/C catalysts showed 2355, 1057, 763, and 772 mA mg^{-1}, respectively, which were decrease of 28.8, 30.0, 44.5, and 41.3% in mass activity, respectively (Figure 5). The higher stabilities of the Pd-Pt alloy UANs and IS NCs are attributed to the Pd-Pt alloy effect, which can effectively suppress the formation of poisoning intermediates and thus maintain clean surfaces during the

9

reactions for long-term.

In summary, the Pd-Pt alloy UANs have been prepared through a facile wet-chemical synthesis. For the formation of UANs, the growth behavior of Pd-Pt nanostructures was modulated by adding optimal concentrations of KI, CTAC, and AA. The I^- ions generated from KI served as a primary ionic capping agent for the preferential 2D growth of Pd and Pt with the passivated {111} plane, and the concentrations of CTAC and AA were adjusted to allow the generation of Pd-Pt alloy UANs in high yield. The Pd-Pt alloy UANs exhibited enhanced EOR catalytic activity and stability compared to Pd-Pt alloy IS NCs, Pd/C, and Pt/C catalysts due to increased active sites by their assembled nanosheet morphology and Pd-Pt alloy composition. This work demonstrates the significance of composition and morphology engineering of nanostructures for potential applications, especially in electrocatalysis.

10

Conflicts of interest

There are no conflicts to declare.

References

[1]   V. Mazumder, Y. Lee, S. Sun, *Adv. Funct. Mater.* **2010**, *20*, 1224-1231.

[2]   J. W. Hong, Y. Kim, Y. Kwon, S. W. Han, *Chem. Asian J.* **2016**, *11*, 2224-2239.

[3]   C. Bianchini, P. K. Shen, *Chem. Rev.* **2009**, *109*, 4183-4206.

[4]   M. K. Kabiraz, J. Kim, W.-J. Lee, B. R. H. C. Kim, S.-U. Lee, J.-R. Kim, S.-M. Paek, J. W. Hong, S.-I. Choi, *Chem. Mater.* **2019**, *31*, 5663−5673.

[5]   S. Guo, S. Zhang, S. Sun, *Angew. Chem. Int. Ed.* **2013**, *52*, 8526-8544.

[6]   J. W. Hong, S. W. Kang, B.-S. Choi, D. Kim, S. B. Lee, S. W. Han, *ACS Nano* **2012**, *6*, 2410-2419.

[7]   M. Liu, Z. Zhao, X. Duan, Y. Huang, *Adv. Mater.* **2019**, *31*, 1802234.

[8]   Z. Qi, C. Xiao, C. Liu, T. W. Goh, L. Zhou, R. Maligal-Ganesh, Y. Pei, X. Li, L. A. Curtiss, W. Huang, *J. Am. Chem. Soc.* **2017**, *139*, 4762-4768.

[9]   Y. Kim, Y. Kwon, J. W. Hong, B.-S. Choi, Y. Park, M. Kim, S. W. Han, *CrystEngComm* **2016**, *18*, 2356-2362.

[10]   P. Chandran, A. Ghosh, S. Ramaprabhu, *Sci. rep.* **2018**, *8*, 3591.

[11]   Y.-Y. Ma, C.-X. Wu, X.-J. Feng, H.-Q. Tan, L.-K. Yan, Y. Liu, Z.-H. Kang, E.-B. Wang, Y.-G. Li, *Energ. Environ. Sci.* **2017**, *10*, 788-798.

[12]   Y. Liu, W. E. Mustain, *J. Am. Chem. Soc.* **2012**, *135*, 530-533.

[13]   K. Persson, A. Ersson, K. Jansson, J. Fierro, S. G. Järås, *J. Catal.* **2006**, *243*, 14-24.

[14]   P. Ciambelli, V. Palma, A. Ruggiero, *Appl. Catal. B Environ.* **2010**, *96*, 18-27.

[15]   W. Yu, M. D. Porosoff, J. G. Chen, *Chem. Rev.* **2012**, *112*, 5780-5817.

[16]   S. Beyhan, J.-M. Léger, F. Kadırgan, *Appl. Catal. B Environ.* **2014**, *144*, 66-74.

[17]   J. W. Hong, Y. Kim, D. H. Wi, S. Lee, S. U. Lee, Y. W. Lee, S. I. Choi, S. W. Han, *Angew. Chem. Int. Ed.* **2016**, *55*, 2753-2758.

[18]   J. Kim, H. Kim, W.-J. Lee, B. Ruqia, H. Baik, H.-S. Oh, S.-M. Paek, H.-K. Lim, C. H. Choi, S.-I. Choi, *J. Am. Chem. Soc.* **2019**, *141*, 18256−18263.

[19]   H. Kim, Y.-D. Ahn, J. Kim, K.-S. Kim, Y. U. Jeong, J. W. Hong, S.-I. Choi, *Chin. J. Catal.* **2020**, *41*, 813-819.

[20]   K. S. Kim, Y. Hong, H. C. Kim, S. I. Choi, J. W. Hong, *Chem. Eur. J.* **2019**, *25*, 7185-7190.

[21]   F. Zhan, T. Bian, W. Zhao, H. Zhang, M. Jin, D. Yang, *CrystEngComm* **2014**, *16*, 2411-2416.

11

[22]   S. E. Habas, H. Lee, V. Radmilovic, G. A. Somorjai, P. Yang, *Nat. Mater.* **2007**, *6*, 692.

[23]   Y. Xia, Y. Xiong, B. Lim, S. E. Skrabalak, *Angew. Chem. Int. Ed.* **2009**, *48*, 60-103.

[24]   W. Li, Y. Deng, Z. Wu, X. Qian, J. Yang, Y. Wang, D. Gu, F. Zhang, B. Tu, D. Zhao, *J. Am. Chem. Soc.* **2011**, *133*, 15830-15833.

[25]   Y. Huang, X.-l. Huang, J.-s. Lian, D. Xu, L.-m. Wang, X.-b. Zhang, *J.Mater. Chem.* **2012**, *22*, 2844-2847.

[26]   C. Yuan, J. Li, L. Hou, X. Zhang, L. Shen, X. W. Lou, *Adv. Funct. Mater.* **2012**, *22*, 4592-4597.

[27]   Y. Pi, N. Zhang, S. Guo, J. Guo, X. Huang, *Nano Lett.* **2016**, *16*, 4424-4430.

[28]   A.-X. Yin, X.-Q. Min, Y.-W. Zhang, C.-H. Yan, *J. Am. Chem. Soc.* **2011**, *133*, 3816-3819.

[29]   Y. Xiong, Y. Xia, *Adv. Mater.* **2007**, *19*, 3385-3391.

[30]   J. W. Hong, M. Kim, Y. Kim, S. W. Han, *Chem. Eur. J.* **2012**, *18*, 16626-16630.

[31]   J. E. Millstone, W. Wei, M. R. Jones, H. Yoo, C. A. Mirkin, *Nano Lett.* **2008**, *8*, 2526-2529.

[32]   Z. Liang, T. Zhao, J. Xu, L. Zhu, *Electrochim. Acta* **2009**, *54*, 2203-2208.

[33]   J. W. Hong, D. Kim, Y. W. Lee, M. Kim, S. W. Kang, S. W. Han, *Angew. Chem. Int. Ed.* **2011**, *50*, 8876-8880.

[34]   H. Xin, S. Linic, *J. Chem. Phys.* **2010**. *132*, 221101-221104.

Accepted Manuscript

12
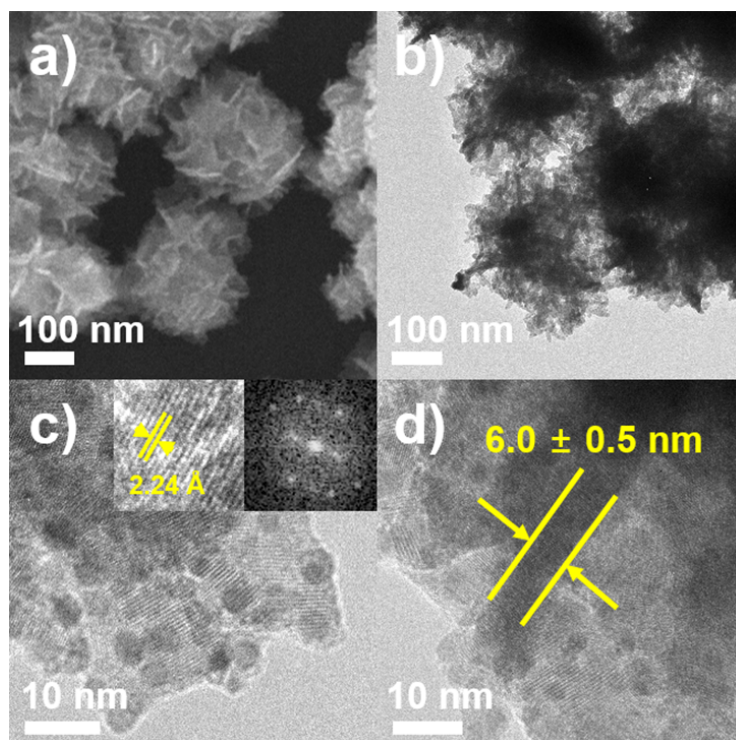
Figure 1. a) SEM, b) TEM, and c) HRTEM images of the Pd-Pt alloy UANs. Insets in (c) showing high-magnification HRTEM image and FFT pattern obtained from a subunit of Pd-Pt alloy UAN. d) HRTEM image of the side face of an ultrathin nanosheet subunit.

13
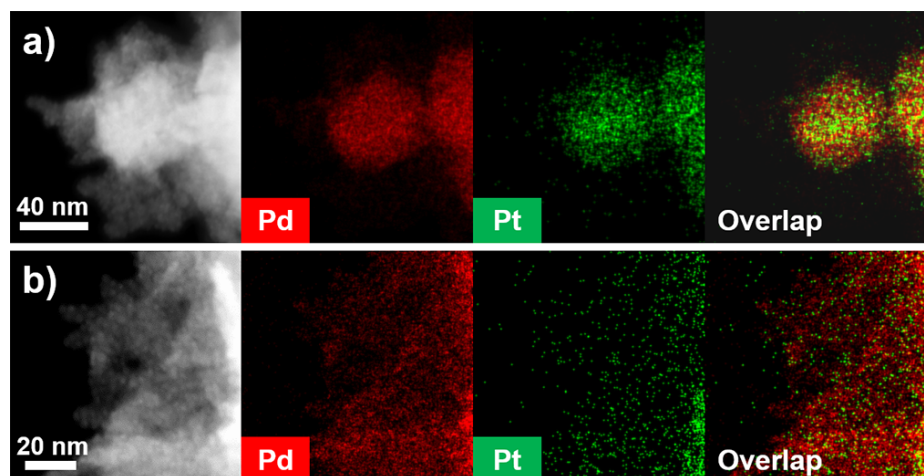
Figure 2. HAADF-STEM image and corresponding EDS elemental maps of a) Pd-Pt alloy UANs and b) ultrathin nanosheet subunit.
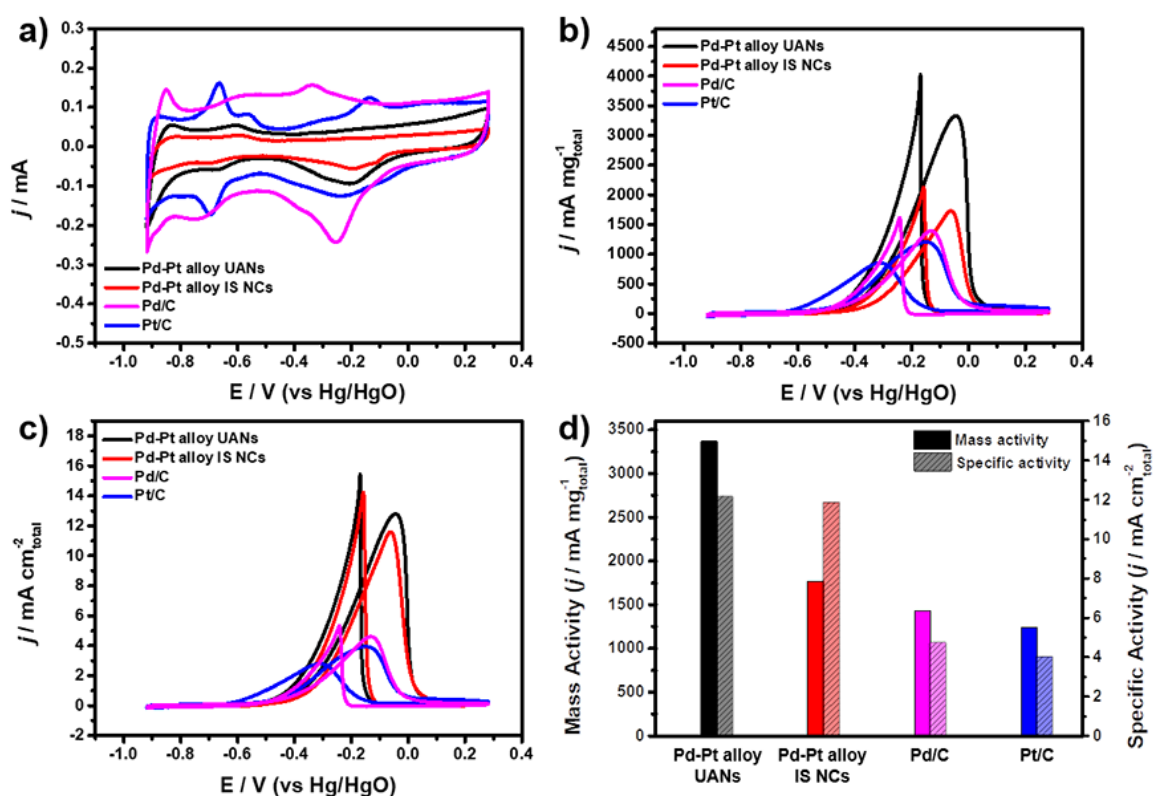
Figure 3. a) CVs of the various catalysts on GCE in 0.5 M KOH and b, c) in 0.5 M KOH + 1.0 M ethanol. The current values were normalized with respect to the b) total metal mass and c) ECSA, respectively and d) corresponding mass activities and specific activities of the various catalysts.

14
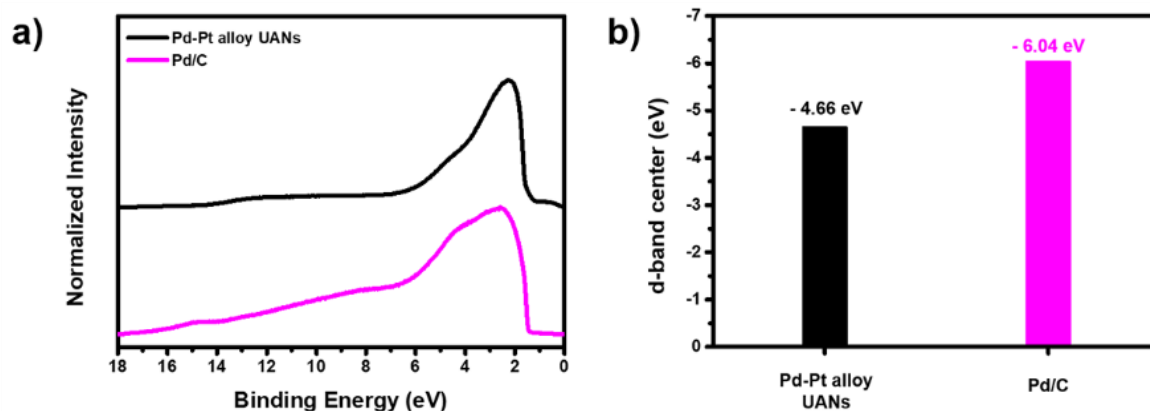
Figure 4. a) XPS spectra for the valence band and b) d-band center positions relative to the Fermi level of Pd-Pt alloy UANs and Pd/C.
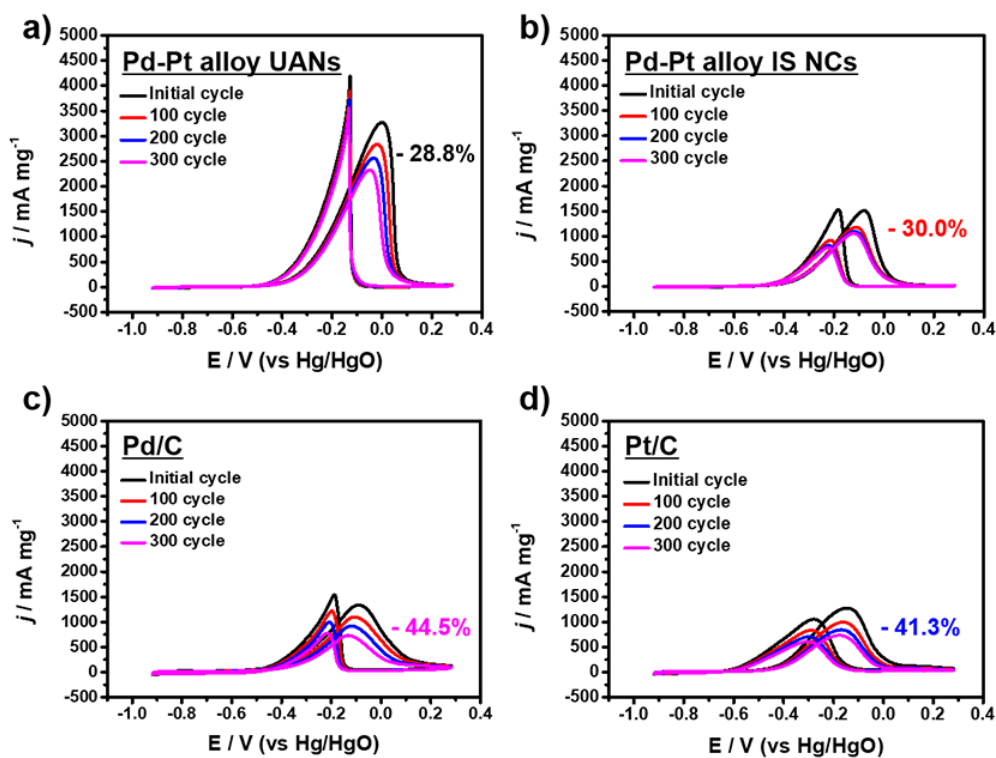
Figure 5. CVs obtained before and after stability test for a) Pd-Pt alloy UANs, b) Pd-Pt alloy IS NCs, c) Pd/C, and d) Pt/C catalysts in 0.5 M KOH + 1.0 M ethanol at a scan rate of 50 mV s^{-1}.

15
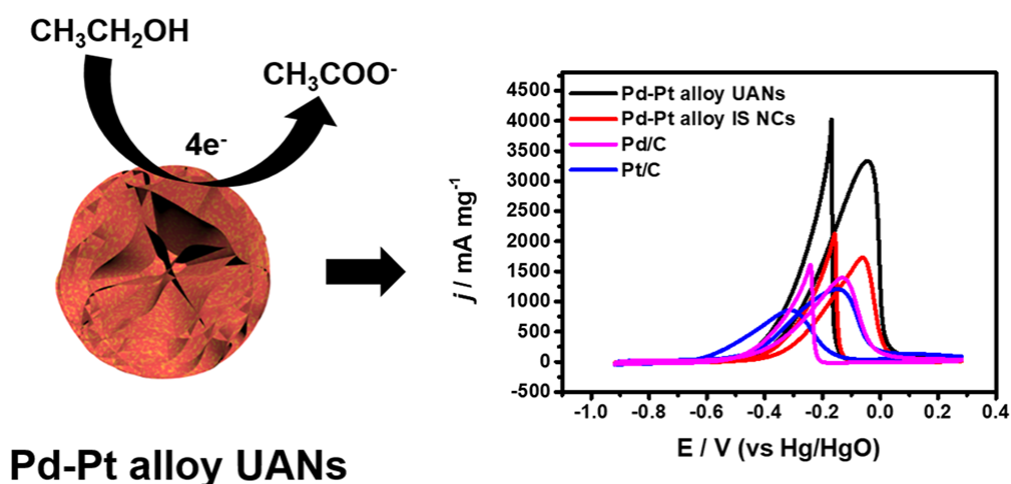
TOC

: Pd-Pt alloy ultrathin assembled nanosheets (UANs) were synthesized by regulating the growth behavior of Pd-Pt nanostructures. The prepared Pd-Pt alloy UANs exhibited the remarkable enhancement of the catalytic activity and stability toward ethanol oxidation reaction (EOR) compared to irregular-shaped Pd-Pt alloy NCs (IS NCs), commercial Pd/C, and commercial Pt/C. This confirms that the Pd-Pt alloy composition and ultrathin 2D morphology offer high accessible active sites and favorable electronic structure for enhancing electrocatalytic activity.

16